RSC Advances

PAPER

View Article Online
View Journal | View Issue

Cite this: *RSC Adv.*, 2026, **16**, 10665

Development of new pyrazole–thiophene hybrids: synthesis, anticancer assessment, and molecular docking insights

Sonia Samy, Samar E. Mahmoud, Ebrahim Abdel-Galil, Ehab Abdel-Latif and Gehad E. Said *

A novel series of pyrazole–thiophene hybrid derivatives (**3a–c**, **5a–c**, **7a–c**, and **9a,b**) was synthesized through a one-step reaction pathway and structurally confirmed by various spectroscopic analyses. Hybridization of the pyrazole nucleus with the thiophene ring was designed to enhance the biological potential of both moieties, as each is known to exhibit diverse pharmacological properties. The MTT assay was used to assess the *in vitro* anticancer potential of the synthesized scaffolds against two human cancer cell lines: hepatocellular carcinoma (HepG2) and breast adenocarcinoma (MCF7). The results indicated that pyrazole–thiophene hybrids **3a** and **5b** demonstrated the highest cytotoxicity against HepG-2 and MCF-7 cells with inhibition values of 24 μM and 10.36 μM and 38.8 μM and 26.9 μM, respectively, compared with the reference drug vinblastine sulfate (8.22 μM for HepG2 and 4.63 μM for MCF-7). Structure–activity relationship (SAR) analysis revealed that the presence of electron-donating substituents on the aromatic ring and thiophene linkage contributed to enhanced cytotoxicity. Molecular docking was conducted to investigate the binding of the compounds to the target protein PDB: 2W3L. The binding free energies for the 2W3L protein ranged between −6.0251 and −7.3575 kcal mol^{-1}, indicating stronger binding compared to vinblastine, which has a binding energy of −5.9584 kcal mol^{-1}. In addition, *in silico* assessment of the pharmacokinetic profile using the SwissADME program showed that compounds **9a** and **9b** appeared as the most promising nominees within the series, demonstrating proper solubility, lower lipophilicity, and, for compound **9a**, high GI absorption. This study presents noteworthy ADME challenges for the series, particularly regarding their solubility and permeability, leading to the need for more synthetic efforts towards more metabolically stable and bioavailable analogues. These findings suggest that pyrazole–thiophene hybrids represent promising scaffolds for the further development of potent anticancer agents.

Received 17th January 2026
Accepted 16th February 2026

DOI: 10.1039/d6ra00429f

rsc.li/rsc-advances

1 Introduction

Uncontrolled cell growth and spread, which can result in invasion of nearby tissues and metastasis to distant organs, are hallmarks of a complex group of disorders known as cancer.[1] Cancer treatment involves a variety of strategies, including surgery, chemotherapy, radiation therapy, and targeted drug therapies aimed at inhibiting proliferation and inducing apoptosis of cancer cells.[2] Drug resistance, severe side effects, and poor selectivity are only a few problems that have been documented in the use of cytotoxic medicines to treat cancer.[3] Thus, ligand-targeted treatment is one of the most promising and tailored approaches to address this problem.[4,5] It aids in the development of more effective medications with numerous mechanisms and selective cytotoxicity to control various types of cancer.[6,7] Liver and breast cancers are among the most common types of cancer globally, with breast cancer being the most frequently diagnosed cancer in women and liver cancer ranking among the top ten common cancers worldwide.[8]

Heterocyclic compounds, especially those containing nitrogen and sulfur, play a vital role in cancer treatment owing to their versatile biological activities and ability to interact with various molecular targets in cancer cells.[9,10] Nitrogen-based heterocycles, such as pyrazole, pyridine, piperidine, indole, and quinazoline, are commonly found in anticancer drugs and are known to inhibit cell proliferation and induce apoptosis through mechanisms such as tyrosine kinase inhibition and regulation of signaling pathways.[11,12] Similarly, sulfur-containing heterocycles, including thiophene derivatives, exhibit significant anticancer properties by targeting kinase receptors and disrupting tumor growth.[13,14] These heterocyclic compounds act by binding to DNA, enzymes, or receptors that are critical for cancer cell survival, leading to cell cycle arrest and apoptosis, making them essential scaffolds for the design of new chemotherapeutic agents.[15,16] The nitrogen and sulfur

Department of Chemistry, Faculty of Science, Mansoura University, 35516 Mansoura, Egypt. E-mail: gehadsaid@mans.edu.eg

atoms in these heterocycles contribute to their chemical reactivity and ability to form hydrogen bonds, thereby enhancing their stability and interactions with cancer-related biomolecules. This has led to the development of several FDA-approved anticancer drugs containing these heterocyclic frameworks, targeting various cancers, including hepatocellular carcinoma and breast cancer.[17,18]

To develop unique molecular structures with a variety of pharmacological activities, heterocyclic hybrids are constructed by combining two or more bioactive heterocyclic scaffolds, each with its own processes. These heterocyclic hybrids are useful chemical probes against a variety of biological targets owing to their adaptable structures, varied biological activities, and capacity to optimize pharmacological qualities.[19] Among heterocyclic compounds containing nitrogen and sulfur with a broad spectrum of pharmacological properties are pyrazoles[20–30] and thiophenes.[31–35] Celebrex, rimonabant, ruxolitinib, antipyrine, deracoxib, and pirtobrutinib are examples of pyrazole derivatives that are included in medications, whereas ticlopidine, teniposide, cefoxitin, raltitrexed, and tiaprofenic acid are examples of thiophene-containing drugs (Fig. 1). Based on the previous mention and given the promising properties of pyrazole and thiophene, our main aim in this research was to synthesize and evaluate the anticancer activity of thiophene scaffolds hybridized with the pyrazole ring system (Fig. 1). The newly synthesized scaffolds were evaluated against two different cancer cell lines. Moreover, computational biology of molecular docking was performed.

2 Results and discussion

2.1 Chemistry

Highly adaptable α-bromoketones have been employed as building blocks to synthesize a variety of heterocyclic scaffolds.[36] Here, we present straightforward and effective methods for the synthesis of some novel pyrazole thienyl ketones *via* the reaction of 2-bromo-1-(5-methyl-1-phenyl-1*H*-pyrazol-4-yl) ethan-1-one (**1**) with various mercapto-phenylamino analogues, building on our earlier work on the synthesis of bioactive heterocyclic compounds under mild conditions.[37,38] 2-Bromo-1-(5-methyl-1-phenyl-1*H*-pyrazol-4-yl)ethan-1-one (**1**), the key analog in our study, was previously prepared through a bromination reaction of 4-acetyl-5-methyl-1-phenylpyrazole,

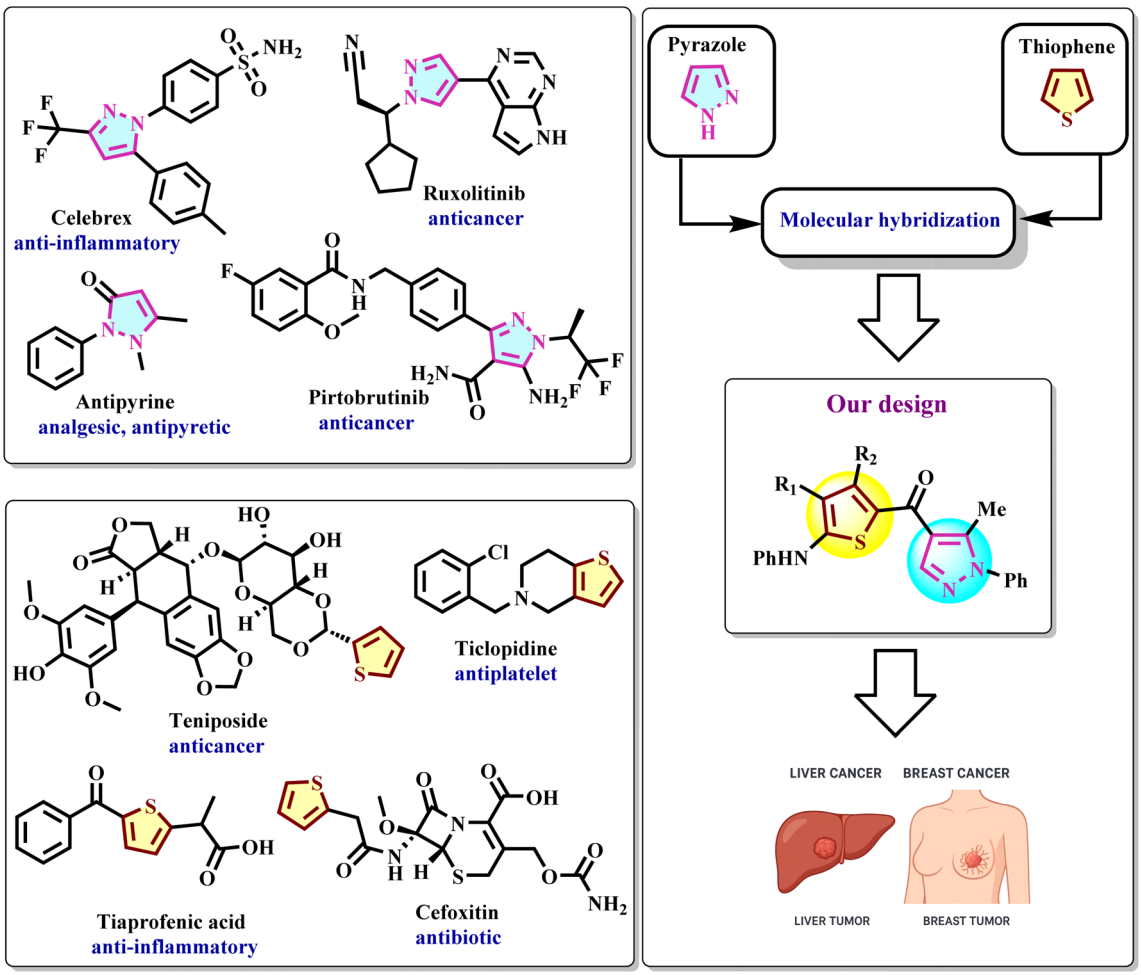

Fig. 1 Some marketed drugs containing pyrazole and thiophene motifs and design approaches for newly synthesized compounds as anticancer agents.

as reported in the literature.[39] In this study, we effectively synthesized a variety of pyrazolyl 3-methylthienyl ketones **3a–c** by heterocyclizing the precursor **1** with 4-anilino-3-arylazo-4-mercapto-but-3-en-2-one derivatives **2a–c**[40] in refluxing ethanol containing a catalytic amount of triethylamine (Scheme 1). Two stages were involved in the construction of the thiophene ring. The first stage involves nucleophilic reaction of the sulfur atom with the α-carbon, transporting the bromide atom to generate intermediate **A**, accompanied by the loss of a hydrogen bromide molecule. The second stage involved a cyclization step through the nucleophilic addition of (–CH_2–) to the carbonyl unit, followed by dehydration. Spectroscopic information represented in IR, ^{1}H NMR, ^{13}C NMR, and mass spectroscopy confirmed the formation of compounds **3a–c**. For example, the IR spectrum of compound **3a** revealed absorption bands at 1650, 1619, and 1595 cm^{-1} characteristic of (C=O), (C=N), and (C=C) functions, respectively. Compound **3a**'s ^{1}H NMR spectrum showed three unique singlet signals for the protons of three methyl groups at δ 2.34, 2.49, and 2.50 ppm.

In a similar way, the equivalent pyrazolyl 3-hydroxythienyl ketones **5a–c** (Scheme 2) were produced by refluxing a mixture of bromoacetyl-pyrazole **1** with ethyl-3-mercapto-3-(phenylamino)-2-(phenyldiazenyl)acrylate scaffolds **4a–c**[41,42] in absolute ethyl alcohol containing triethylamine as a catalyst. The thiophene motif was formed through a nucleophilic substitution reaction of the bromine atom in compound **1** with the –SH from the thiocarbamoyl moiety (intermediate **B**), accompanied by the elimination of an ethanol molecule. The spectral and elemental data of the ascribed molecular structures **5a–c** were entirely compatible. The IR spectra of compounds **5a–c** showed characteristic stretching vibration bands of the carbonyl group at lower frequencies of 1606, and 1596 cm^{-1}, respectively. Intramolecular hydrogen bonds between the hydroxyl and carbonyl groups were thought to be responsible for this. The protons of the methyl and methoxy groups (pyrazole ring and phenyl ring) were identified by two singlet signals at δ 2.51 and 3.83 ppm in the up-field area of the ^{1}H NMR spectrum of compound **5b**. Additionally, the proton of the NH function showed a singlet signal at 12.40 ppm. Also, the formula $C_{28}H_{23}N_5O_3S$ was validated by the mass spectrometry, which showed the base peak at (m/z = 509, M^+).

Into our target to synthesize various thiophene rings linked to the pyrazolyl ketone, pyrazolyl 3-aminothienyl ketones **7a–c** were prepared by agitating the bromoacetyl-pyrazole **1** with 2-cyano-3-mercapto-*N*-phenyl-3-(phenylamino)acrylamide derivatives **6a–c**[43] in dry *N*,*N*-dimethylformamide and potassium carbonate for five hours at 25 °C (Scheme 3). Spectroscopic and elemental information verified the formation of products **7a–c**, likely produced *via* intermediate **C**, which underwent intramolecular addition of a methylene group (–CH_2) to the nitrile group (–CN) to give the proposed pyrazolyl 3-aminothienyl ketones **7a–c**. For example, compound **7a** revealed distinctive absorption bands at 3441 and 3278 cm^{-1} due to (NH_2, 2NH) functions and 1655 and 1630 cm^{-1} due to (2C=O) functions in its IR spectrum. ^{1}H NMR assigned four singlet signals at 2.26, 2.52, 9.37, and 11.59 ppm for ($2CH_3$), (NH_2), and (NH) groups protons. In addition, mass spectrometry revealed a base peak at (m/z = 507, M^+), validating the formula $C_{29}H_{25}N_5O_2S$.

In an identical way to compounds **3a–c**, when bromoketone **1** was allowed to react with the mercapto(phenylamino)methylene derivatives **8a,b**[44] under the same conditions, it yielded the targeted pyrazole 3-methylthienyl ketones **9a,b** (Scheme 4). The reaction mechanism involves a nucleophilic substitution reaction of the bromide atom in compound **1** by the sulfur atom in compound **8** and losing a hydrogen bromide molecule, followed by an intramolecular cyclization step in intermediate **D** accompanied by dehydration of a water molecule. Both spectral and analytical data clarified the structures of compounds **9a** and **9b**, which matched the suggested molecular structures (see Experimental section). Three absorption bands at (ν = 3111, 1640, 1608 cm^{-1}) in the infrared spectrum of pyrazole 3-methylthienyl ketone **9a** were identified as belonging to the NH and two C=O groups, respectively. Additionally, four singlet signals at δ = 2.46, 2.58, 2.63, and 11.59 ppm in the ^{1}H NMR

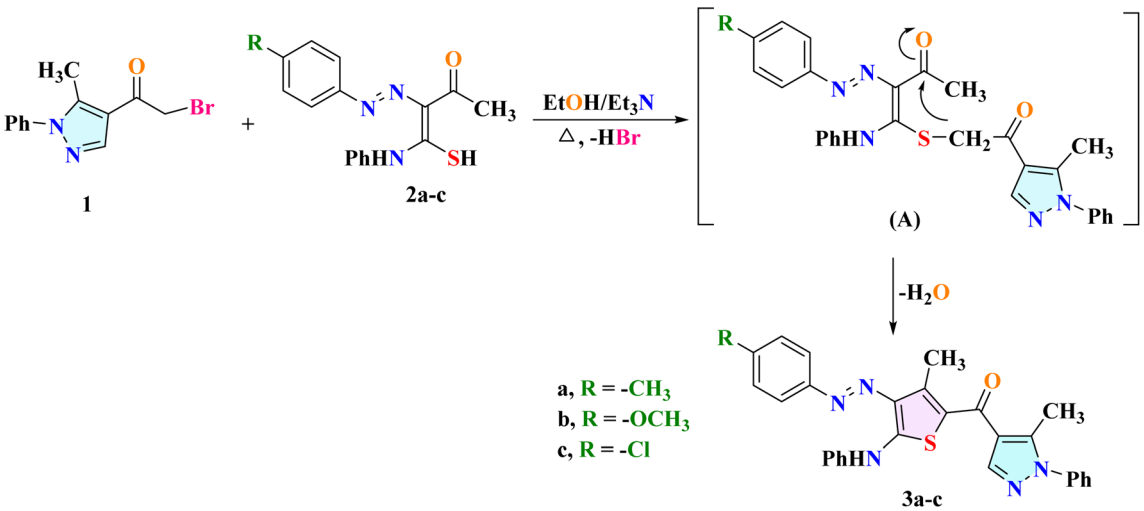

Scheme 1 Synthesis of pyrazole 3-methylthienyl ketones **3a–c**.

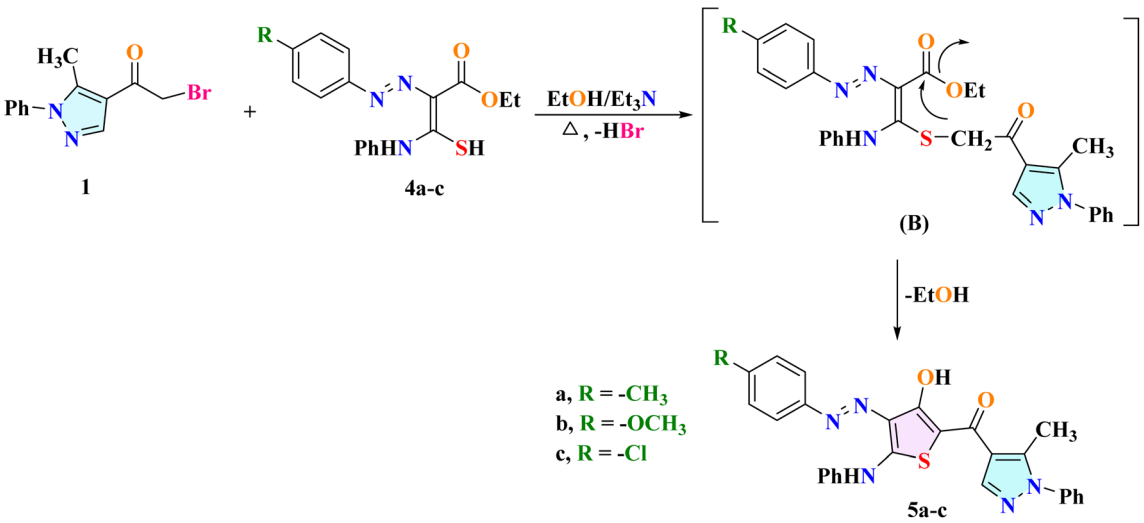

Scheme 2 Synthesis of pyrazole 3-hydroxythienyl ketones **5a–c**.

spectrum were identified as representing the protons of three CH_3 and NH groups. Additionally, the base peak ($m/z = 415$, M^+) in the MS spectrum supported the molecular formula $C_{24}H_{21}N_3O_2S$.

2.2 Nitrosamine risk assessment

Considering the presence of a pyrazole scaffold and the use of triethylamine and *N*,*N*-dimethylformamide in the synthetic route, a nitrosamine risk assessment was conducted. Although these reagents may represent potential sources of amine-related impurities, the applied synthetic conditions were maintained under neutral to basic environments and did not involve nitrosating agents or acidic conditions known to promote nitrosamine formation. Accordingly, the probability of nitrosamine generation during the synthesis of the pyrazole–thiophene hybrids is considered negligible.

2.3 Impurity profile and toxicological consideration

The impurity profile of the proposed synthetic route was evaluated based on the reaction design, reagents, and purification steps. The potential impurities are expected to be limited to unreacted starting materials, minor side products, and residual solvents or reagents, including triethylamine and *N*,*N*-dimethylformamide. These impurities were effectively removed during purification, as confirmed by TLC monitoring, NMR spectral analysis, and elemental analysis of the final compounds.

2.4 Biological activity

2.4.1 Anticancer activity. The cytotoxic potential of the synthesized compounds **3a–c**, **5a–c**, **7a–c**, and **9a,b** was evaluated against two mutant human cancer cell lines, HepG2 (hepatocellular carcinoma) and MCF-7 (breast

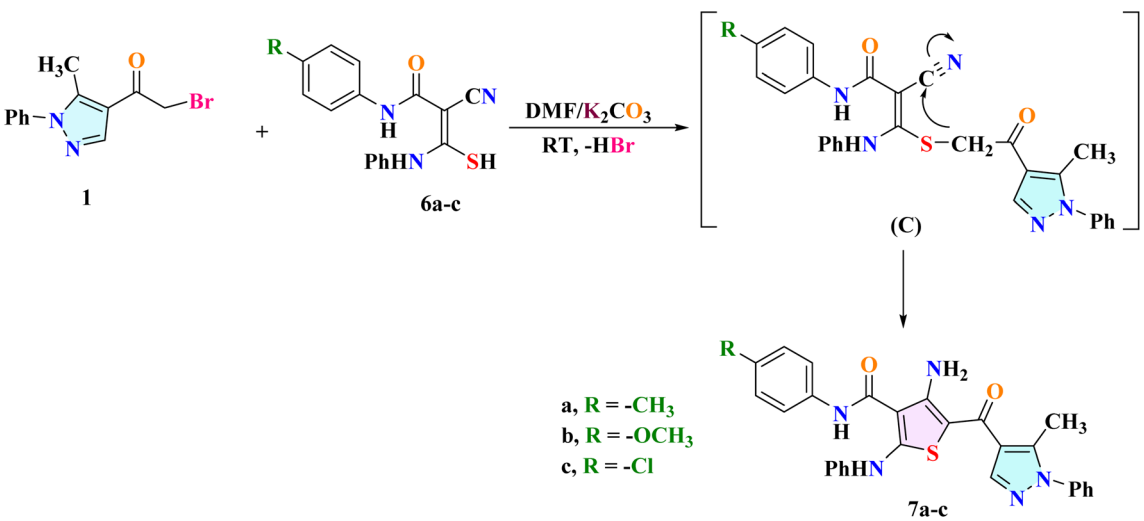

Scheme 3 Synthesis of pyrazole 3-aminothienyl ketones **7a–c**.

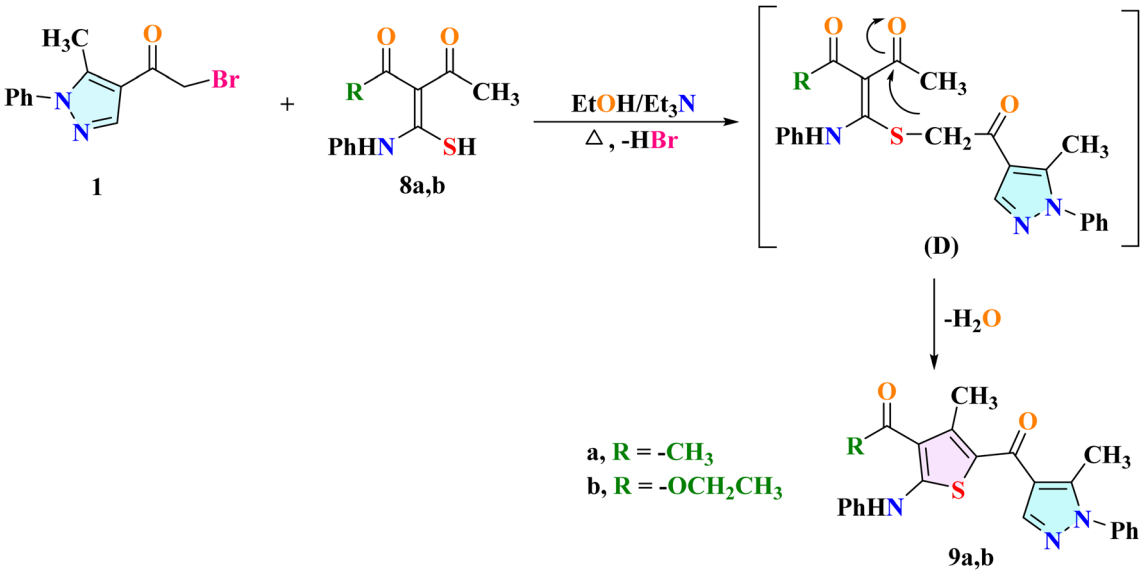

Scheme 4 Synthesis of pyrazole 3-methylthienyl ketones **9a,b**.

adenocarcinoma), using the MTT colorimetric assay and vinblastine sulfate as the reference drug. The speed, precision, and capacity of this assay to screen a large number of cell lines make it a useful technique for evaluating the efficacy of new cytotoxic drugs. Table 1 summarizes the data. The average inhibitory concentration (IC_{50}), which inhibits 50% of the biological activity of cells, was used to determine the cytotoxicity of the compounds under investigation. For comparison purposes, the inhibitory activity of the evaluated compounds is illustrated in graphic plots of the growth inhibition percentages at 500 μM against the compounds (Fig. 2). All tested compounds exhibited variable inhibitory effects on both cell lines. Notably,

Table 1 IC_{50} (μM) of the newly synthesized hybrids against HepG2 and MCF7 cell lines

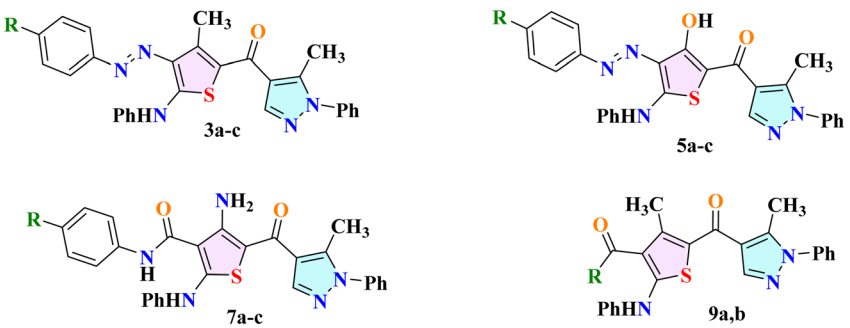

		In vitro cytotoxicity IC_{50} ± SD (μM)	
Compound no.	R	HepG2	MCF7
3a	CH_3	24 ± 1.03	10.36 ± 0.37
3b	OCH_3	>100	>100
3c	Cl	>100	>100
5a	CH_3	>100	59.7 ± 0.21
5b	OCH_3	38.8 ± 2.36	26.9 ± 0.43
5c	Cl	77.6 ± 1.48	49.4 ± 1.76
7a	CH_3	>100	99.0 ± 1.38
7b	OCH_3	>100	55.2 ± 0.73
7c	Cl	85.7 ± 0.73	49.0 ± 0.94
9a	CH_3	>100	>100
9b	OCH_2CH_3	>100	>100
Vinblastine sulfate	—	8.22 ± 0.44	4.63 ± 0.66

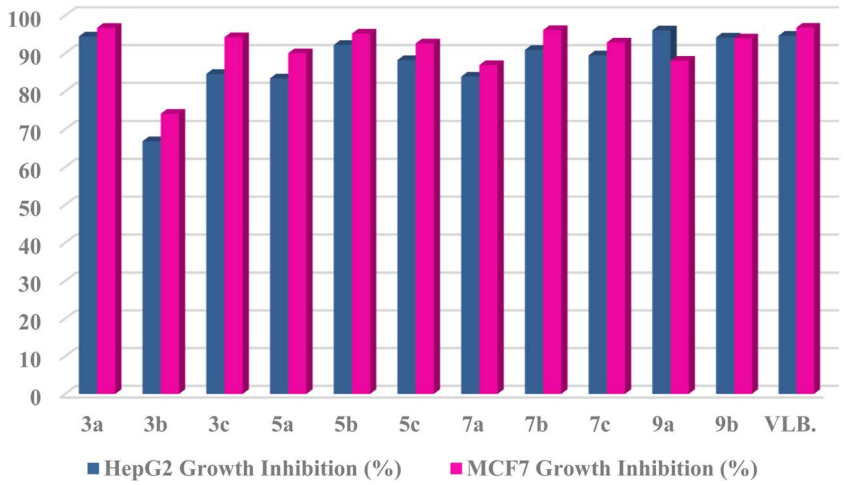

Fig. 2 Cytotoxic activities of compounds **3a–c**, **5a–c**, **7a–c**, and **9a,b** against HepG-2 and MCF-7 cancer cells.

compound **3a** demonstrated the highest cytotoxic activity against both cancer cell lines out of all the compounds that were examined. It displayed an IC_{50} value of 10.36 μM against MCF-7 and 24 μM against HepG2, placing it in close range of the reference drugs vinblastine sulfate (4.63 μM for MCF-7, 8.22 μM for HepG2), doxorubicin (4.17 μM for MCF-7, 4.50 μM for HepG2),[45] erlotinib (8.20 μM for MCF-7, 7.73 μM for HepG2),[45] and sorafenib (7.26 μM for MCF-7, 9.18 μM for HepG2).[45] These results highlight compound **3a** as a promising pyrazole–thiophene multitargeted anticancer lead, offering potential for further optimization to overcome hepatocellular and breast carcinoma in cancer therapy.

Following that, compound **5b** demonstrated considerable activity (26.9 μM and 38.8 μM) against MCF-7 and HepG-2 cells. Compounds **5c** and **7c** showed moderate effects against HepG-2 cells with inhibition values of 77.6 μM and 85.7 μM, respectively. Compounds **5a**, **5c**, **7b**, and **7c** showed moderate effects against MCF-7 cells with inhibition values of 59.7 μM, 49.4 μM, 55.2 μM, and 49.0 μM, respectively. Against these two cell lines, compounds **3b**, **3c**, **7a**, **9a**, and **9b** demonstrated extremely poor growth inhibition. Additionally, compounds **5a** and **7b** demonstrated no discernible cytotoxic effect in hepatocellular carcinoma cell lines. Notably, breast cancer cells displayed the lowest IC_{50} values, whereas hepatocellular cancer cells displayed the highest IC_{50} values.

In order to establish the biological activity of the newly synthesized pyrazole–thiophene hybrids, the cytotoxicity of the newly synthesized compounds has been compared to some of the most used chemotherapeutic agents, such as doxorubicin, which is used to treat estrogen receptor-positive breast cancer, including MCF-7, and sorafenib, used to treat hepatocellular carcinoma. As expected, the reference compounds have shown higher activity than the newly synthesized compounds, which is a natural consequence of the level of optimization and advancement of the compounds under study. However, the newly synthesized compounds have to be regarded as first-generation compounds, as they contain two privileged structures, *i.e.*, pyrazole and thiophene. Significantly, several compounds were found to exhibit moderate yet significant cytotoxicity against the MCF-7 and HepG2 cell lines, validating the rationale behind the hybridization strategy employed in the study. Although the IC_{50} values of the compounds are high when compared to the IC_{50} values of established chemotherapeutic agents, the framework presents a wide scope for further optimization and refinement. This could involve rational substitution with electron-withdrawing groups to increase the binding affinity, adjustments to the lipophilicity to increase membrane permeability, and strategic incorporation of additional hydrogen-bonding centers to increase the binding affinity, as indicated by molecular docking analysis. Although the compounds are not as potent as the current standard treatment regimens, they present a promising platform from which further refinement and optimization could result in even more potent and potentially safer therapeutic agents.

2.5 Structure–activity relationship (SAR) studies

A new set of unique pyrazolylthiophene hybrids was synthesized using a hybridization technique. In a variety of cancer cell lines, pyrazole derivatives hybrid with thiophene motif have been demonstrated to suppress cell growth and cause cell cycle arrest.[46] Using bromoacetyl-pyrazole **1** as a starting precursor, the test compounds are mapped into four structural profiles: **A** (**3a–c**), **B** (**5a–c**), **C** (**7a–c**), and **D** (**9a,b**) (Fig. 3).

By inspection of the experimental data of the anticancer activity of the newly synthesized hybrids, the following structural activity relationship assumptions are proposed.

In comparison to vinblastine sulfate, the recorded data verified that pyrazolyl 3-methylthienyl ketone **3a** was the most effective derivative in group **A** against HepG2 (hepatocellular carcinoma) and MCF-7 (breast adenocarcinoma) cells, with IC_{50} values of 24 and 10.36 μM, respectively. Interestingly, the insertion of a hydrophilic electron-donating group ($-CH_3$) in the para position to the phenyl ring may greatly boost the anticancer action.[47] On the other hand, switching from *p*-CH_3 in **3a** to $-OCH_3$ in **3b** and –Cl in **3c** decreased the growth inhibition to a great extent.

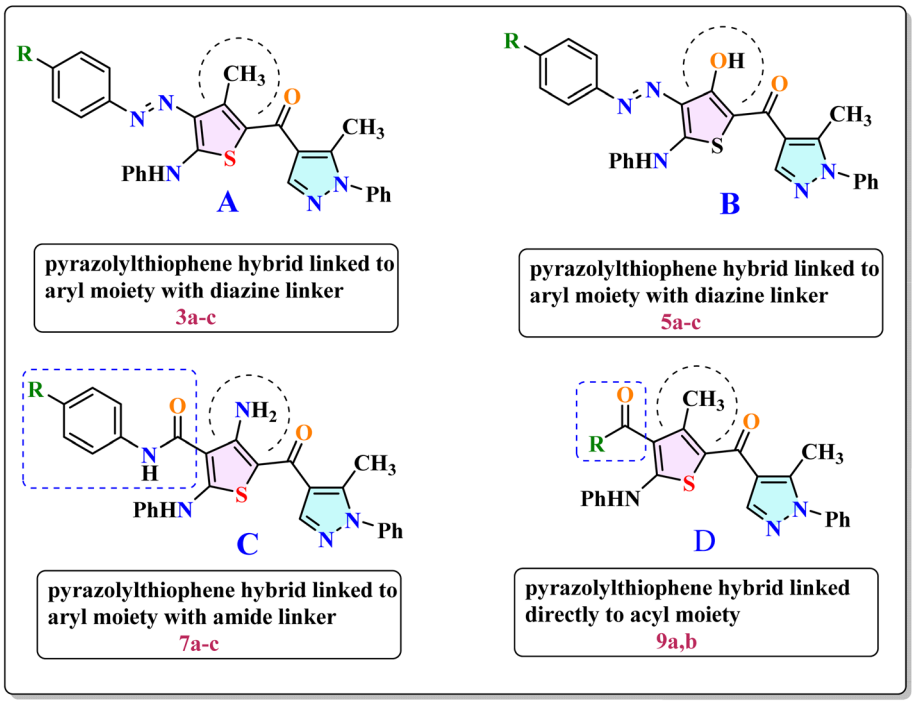

Fig. 3 Structural profile map of the tested pyrazolylthiophene compounds.

Regarding the second group, **B**, the pyrazolyl 3-hydroxythienyl ketone **5b** exhibited higher growth inhibition than pyrazolyl 3-hydroxythienyl derivatives **5a** and **5c** against HepG2 and MCF-7 cells with IC_{50} values of 38.8 and 26.9 μM, respectively. By rendering the molecule more lipophilic and capable of forming hydrogen bonds with significant residues in the active site, the insertion of a hydrophilic electron-donating group, such as a methoxy group (–OCH_3) into the para position of the phenyl ring with a hydroxyl group (–OH) linked to the thiophene ring, could significantly enhance anticancer activity. Noticeably, when the *p*-OCH_3 group in compound **5b** was switched to *p*-Cl in compound **5c**, a concomitant slight decrease in anticancer activity against HepG2 and MCF-7 cells was noted (IC_{50} = 77.6 and 49.4 μM).

Group **C** (compounds **7a–c**) demonstrated the vital role of the diazine linker. Significantly, connecting the aryl moiety and the pyrazolylthiophene hybrid through an amide linker adversely affected the anticancer activity against HepG2 cells. Because of the presence of a chlorine nucleus as a branch on the phenyl ring of the azo moiety,[48] compound **7c** exhibited a small improvement in the activity against HepG2 and MCF-7 cells with IC_{50} values of 85.7 and 49.0 μM, respectively.

Also, the SAR study illustrated the negative effect of the acyl group directly linked to the thiophene ring in group **D** (compounds **9a,b**) on the anticancer activity against both HepG2 and MCF-7 cells.

2.6 Molecular docking

The B-cell lymphoma-2 protein was selected owing to its contribution in the regulation of apoptosis and has a vital role of the protein in the survival and chemoresistance of malignance cells. However, Bcl-2 is one of antiapoptotic proteins elaborated in the destruction of mitochondrial outer membrane permeability, hence hindering cytochrome-c release and caspase activation. Also, Bcl-2 has been concerned in a number of tumors, including both hepatocellular carcinoma and breast adenocarcinoma, where it contributes to tumor growth and adds to resistance in contradiction of conventional chemotherapy drugs. The molecular docking was employed to predict the different modes and affinities of the synthesized pyrazole thienyl ketones toward the target PDB: 2W3L active site (Table S2 and Fig. 4). Among all pyrazole thienyl ketones, pyrazole 3-aminothienyl ketone **7c** unveiled the highest score of binding (−7.3575 kcal mol^{-1}), strong binding through H-acceptor, and two π–cation stackings with Arg66, Arg68, and Arg105 over 3.35, 3.53, and 3.71 Å, respectively, signifying high stability inside the targeted pockets. The pyrazole 3-aminothienyl ketone **7a** demonstrated prominent affinity (−7.1000 kcal mol^{-1}) through H-acceptor bonding between the O7 atom of the amide group and Arg105 (3.33 Å), H–π stacking between the C26 atom of the phenyl ring with Phe71 (4.45 Å), π–cation stacking between the pyrazole ring and Arg66 (4.02 Å), and H–π stacking between the aniline ring and Gly104 (3.59 Å). While the pyrazole 3-aminothienyl ketone **7b** established lower affinity (−6.8632 kcal mol^{-1}) through π–H stacking between the aniline ring and Arg68 (3.64 Å). Meanwhile, the pyrazole 3-hydroxythienyl ketones **5a–c** showed reliable binding scores between −6.2690 and −6.6810 kcal mol^{-1}, stabilized mainly through π–H, π–cation stackings, and hydrogen donor interaction with Glu119, Ala72, Tyr67, and Arg66 amino acids, over intermolecular distances between 2.88 and 4.25 Å. In particular, **5c**

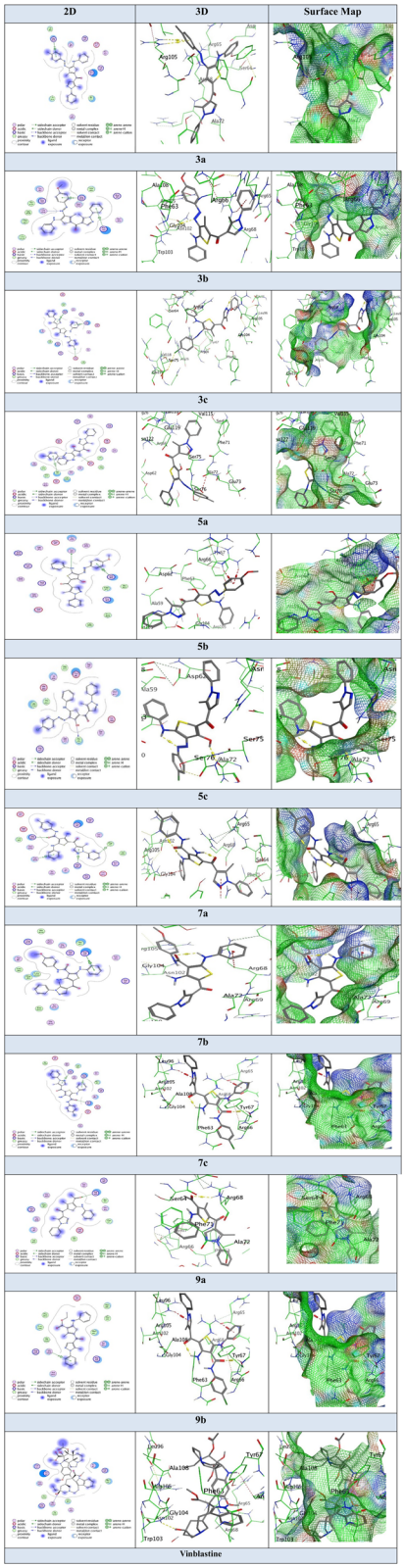

Fig. 4 Docking images of the synthesized pyrazole thienyl ketones and vinblastine reference drug.

exhibited a proper hydrogen donor bond between the O8 atom of the hydroxyl group with Ala72, implying the smallest intermolecular distance (2.88 Å). Moreover, the pyrazole 3-methylthienyl ketones **3a–c** demonstrated significant π–cation stackings, especially between the aromatic and heteroaromatic rings such as phenyl, anisyl, aniline, and pyrazole rings and Arg105 and Arg68. Remarkably, pyrazole 3-methylthienyl ketone **3c** (−6.8042 kcal mol^{-1}) showed double π–cation interactions with Arg105, and Arg86 enhancing its stabilization within the target PDB: 2W3L active site. Moreover, the pyrazole 3-methylthienyl ketones **9a** and **9b** maintained weak bindings (−6.1589 and −6.0251 kcal mol^{-1}, respectively). However, the pyrazole 3-methylthienyl ketone **9a** formed one hydrogen acceptor between the Arg68 and the O1 atom of the acetyl group, while analogue **9b** involved one π–H stacking between Gly104 and its phenyl ring. These results represented the importance of electronic and spatial structures in determining optimal binding. Overall, the docking results demonstrated that structural distinctions, mostly involving toluene, thiophene, and pyrazole moieties, significantly influenced the interaction forms and binding scores. The enhanced bindings relative to vinblastine (reference) suggest potential biological relevance and rationalize additional *in vitro* and *in vivo* assessment of these analogues.

The various docking positions indicate significant variations in the orientations and modes of these synthesized compounds towards interacting with the binding groove of Bcl-2. Compounds with hydrogen-bonding functionalities, such as amide or alcoholic groups, tend to be oriented towards interacting with polar amino acid residuals in the BH3 binding site, hence enabling them to bind strongly with interactions at these groups. The remaining compounds with non-polar functionalities tend to have various orientations in their bindings that tend to be focused on π–cationic or π–H interactions with basic patches, such as arginine-rich regions, within the binding cleft. However, the various aromatic substitution showed an influence on the ligand through the hydrophobic regions in the pocket. In addition, electron-donating substituents displayed good π-stacking interactions with the aromatic residues, whereas larger or less flexible substituents induced steric hindrance, resulting in diverse binding geometries and reduced stabilization. These explain the diversity in binding mode observed among the synthesized derivatives and underpin how subtle structural changes control ligand–protein complementarity. Overall, this docking analysis has established that a balance between hydrogen bonding capability, aromatic surface area, and conformational flexibility is responsible for the differential binding behavior exhibited by compounds toward Bcl-2, furnishing a molecular basis for their variable biological activities.

2.7 Pharmacokinetic character

Insight into the pharmacokinetic profile based on the SwissADME prediction: compounds **3a–c** displayed low GI absorption, non-BBB permeants, high lipophilicity (log *P* ranged from 6.24 to 6.77), and large molecular weight resulting in poor solubility across all prediction models (ESOL solubility = 10^{-6} mg mL^{-1}). Chlorinated derivative **3c** showed more lipophilicity and solubility, depending on the presence of

a hydrophobic halogen. All compounds **3a–c** debased multiple drug-likeness filters (Ghose, Muegge) and presented alerts for pan-assay interference (PAINS), raising concerns about potential false-positive activity in biochemical assays (Table S3 and Fig. 5). Alongside series **5a–c**, which differed from compounds **3a–c** by the presence of the hydroxyl group on the thiazole ring, showed an improvement in solubility and a minor decrease in lipophilicity, as in compound **5b** (log P = 5.65). Notwithstanding, the profiles remained poor, with low GI absorption, no BBB penetration, and poor solubility. However, the increase in the H-donor bonds in this series resulted in low permeability. Compound **5b** appeared to be an inhibitor of CYP2C9, indicating a probable for drug–drug interaction. Similar to compounds **3a–c**, these compounds carried PAINS indication and multiple drug-likeness violations. Meanwhile, compounds **7a–c** contain an amide group in their structures, revealed a decrease in the lipophilicity (log P ranged from 4.82 to 5.34) and a corresponding improvement in the solubility, as in compound **7b** (ESOL solubility = 2.68×10^{-5} mg mL^{-1}). However, the GI absorption remained low, with a topological polar surface area (TPSA > 130 $Å^2$) and increased H-bonding capacity. So, the prediction of inhibition against CYP2C19 and CYP2C9 for all derivatives, and CYP2D6 for compounds **7a** and **7b**, showed a significant risk for metabolic interactions. Thus, this series displayed free of PAINS remarks and a confident feature for additional development. Moreover, compounds **9a** and **9b**, lacking both the aniline and hydrazone/amide linker present in the other series, exhibited the more constructive ADME profiles within the set. They demonstrated lower molecular weights and lipophilicity (log P = 4.83). Importantly, compound **9a** established high GI absorption, a unique feature in this series. It showed the best aqueous solubility profiles (highly soluble) and complied with Lipinski's and Veber's rules. While it inhibits CYP2C9 and CYP3A4, its overall properties make it the most feasible lead for more optimization.

While compounds **9a** and **9b** showed the best docking scores and the most promising ADME and drug-likeness profiles, their cytotoxicity towards the HepG2 and MCF-7 cancer cells was relatively low. This again underlines the fact that the best *in silico* pharmacokinetic parameters and the best docking scores do not necessarily predict the best antiproliferative activity. It should be emphasized that the SwissADME package is used to predict the drug-likeness and the pharmacokinetic parameters of compounds, and not their biological activity. In the same way, the docking study is used to predict the binding ability of compounds to a target under ideal conditions and does not consider the complex biological processes involved in the activity of compounds. In fact, the biological activity of compounds is influenced by a series of complex biological parameters, including the uptake of compounds by the cells, their efflux, metabolic stability, and other pharmacodynamic parameters. It is for this reason that, although compounds **9a** and **9b** can be regarded as lead-like and pharmacokinetically interesting, compounds **3a** and **5b** showed more potent experimental cytotoxicity profiles. This is a demonstration of the complementary relationship as opposed to the predictive relationship between *in silico* studies and experimental studies. It is also a demonstration that more work is needed to balance pharmacokinetic favorability and biological activity.

3 Experimental

3.1 Materials and instruments

Dry solvents were used for all chemical reactions. The purity of the obtained products and the time of the chemical reactions were tracked by thin-layer chromatography (TLC) on silica gel plates using an eluent (P.E. and E.A.). The visualizing agent was a UV lamp. The GALLENKAMP apparatus was used to record the melting points (m.p.). The FTIR Spectrometer, INVENIO S, Bruker, was used to measure infrared spectra (IR). JEOL's spectrometer (500 and 125 MHz) was used to perform NMR spectra (^{1}H-NMR and ^{13}C-NMR) using DMSO-d_6. A PerkinElmer 2400 analyzer and a Thermo Fisher Scientific GC/MS model DSQ II were used to obtain elemental (C, H, and N) and mass analyses, respectively.

3.2 Synthesis of pyrazole 3-methylthienyl ketones 3a–c

A solution of 4-mercapto-4-(phenylamino)-3-(phenylazo)but-3-en-2-one derivative **3a**, **3b**, or **3c** (5 mmol) in 25 mL ethyl alcohol and a catalytic amount of triethylamine (3 drops) was mixed with bromoacetyl-pyrazole **1** (1.40 g, 5 mmol) in a 50 mL single-neck round-bottomed flask. After four hours of refluxing, the mixture was allowed to cool to 30 °C. The corresponding pyrazole-thienyl derivatives **3a–c** were obtained by filtering and recrystallizing the colorful product from the EtOH/DMF mix (5 : 1).

3.2.1 (*E*)-(5-Methyl-1-phenyl-1*H*-pyrazol-4-yl)(3-methyl-5-(phenylamino)-4-(*p*-tolyldiazenyl)thiophen-2-yl)methanone (3a). Yield = 70.5% (pale red); m.p. = 208–210 °C. IR: 3265 (NH), 1650 (C=O), 1619 (C=N), 1595 (C=C) cm^{-1}. ^{1}H NMR δ: 2.34 (s, 3H, CH_3), 2.49 (s, 3H, CH_3), 2.50 (s, 3H, CH_3), 7.26 (t, J = 7.50 Hz, 1H), 7.29 (d, J = 8.00 Hz, 2H), 7.45 (d, J = 8.00 Hz, 2H), 7.50 (t, J = 7.00 Hz, 3H), 7.55–7.59 (m, 4H), 7.64 (d, J = 8.00 Hz, 2H), 8.14 (s, 1H, pyrazole-H), 13.72 (s, 1H, NH). ^{13}C NMR δ: 11.44, 13.53, 20.43, 107.38, 118.22 (3C), 120.53 (3C), 120.93, 125.11 (3C), 125.44, 129.11 (3C), 129.49 (3C), 129.79 (2C), 139.96, 140.93 (2C), 143.90, 144.83, 181.83. Mass analysis (*m*/*z*, %): 491 (M^+, 41), 103 (43), 101 (40), 85 (27), 69 (22), 57 (42), 53 (26), 86 (100). Analysis for $C_{29}H_{25}N_5OS$ (491.18): calculated: C, 70.85; H, 5.13; N, 14.25. Found: C, 70.92; H, 5.09; N, 14.29%.

3.2.2 (*E*)-(4-((4-Methoxyphenyl)diazenyl)-3-methyl-5-(phenylamino)thiophen-2-yl)(5-methyl-1-phenyl-1*H*-pyrazol-4-yl)methanone (3b). Yield = 78.4% (dark red); m.p. = 223–225 °C. IR: 3255 (NH), 1650 (C=O), 1619 (C=N), 1595 (C=C) cm^{-1}. ^{1}H NMR δ: 2.48 (s, 3H, CH_3), 2.59 (s, 3H, CH_3), 3.83 (s, 3H, OCH_3), 7.07 (d, J = 8.50 Hz, 2H), 7.23–7.25 (m, 1H), 7.46–7.52 (m, 5H), 7.56 (d, J = 5.00 Hz, 4H), 7.79 (d, J = 9.00 Hz, 2H), 8.10 (s, 1H, pyrazole-H), 13.13 (s, 1H, NH). Mass analysis (*m*/*z*, %): 507 (M^+, 27), 389 (12), 327 (56), 301 (73), 286 (25), 276 (51), 143 (37), 76 (42), 69 (51), 44 (73), 43 (75), 42 (57), 252 (100). Analysis for $C_{29}H_{25}N_5O_2S$ (507.17): calculated: C, 68.62; H, 4.96; N, 13.80. Found: C, 68.70; H, 5.00; N, 13.71%.

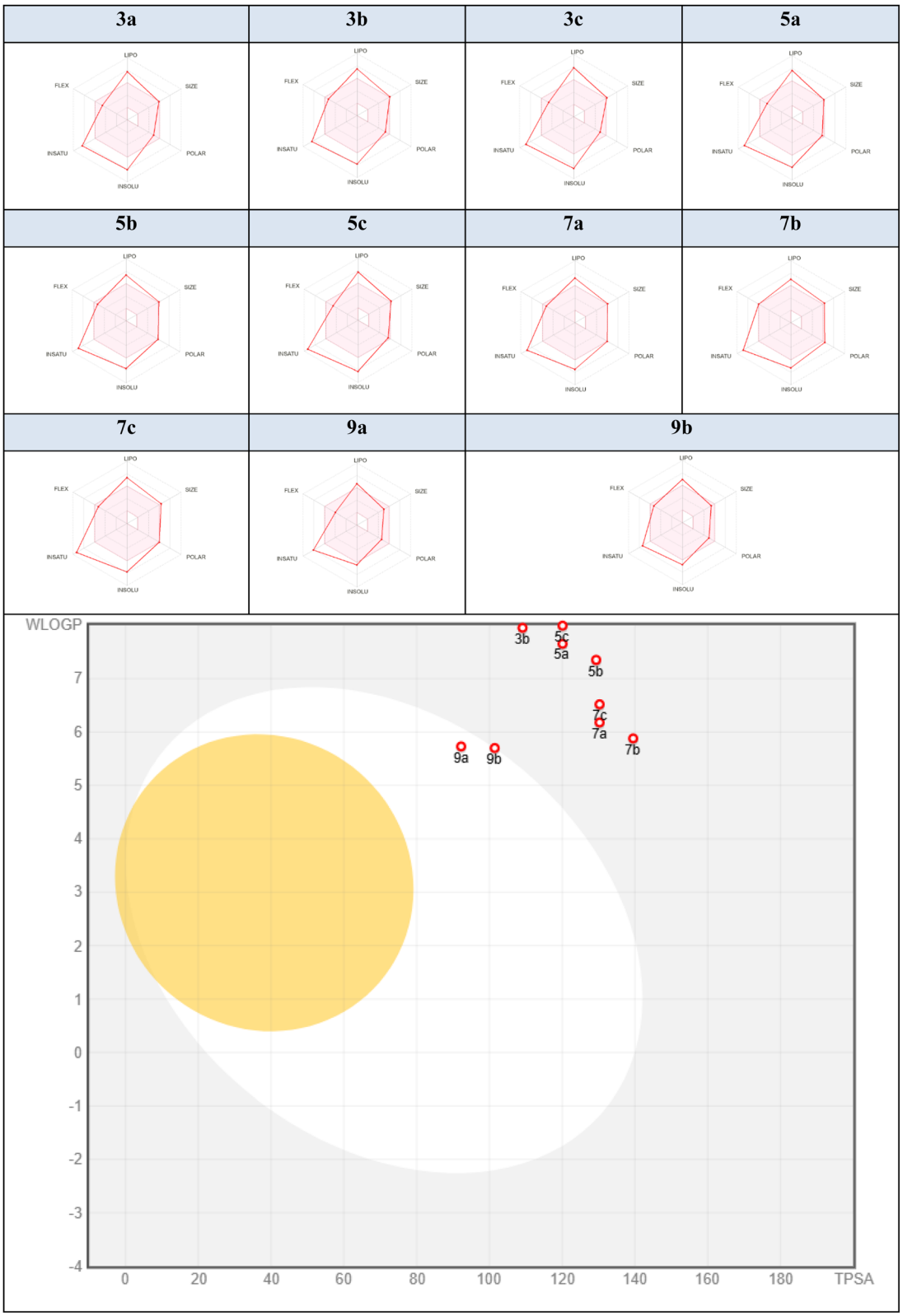

Fig. 5 Radar charts and boiled eggs of the synthesized compounds.

3.2.3 (*E*)-(4-((4-Chlorophenyl)diazenyl)-3-methyl-5-(phenylamino)thiophen-2-yl)(5-methyl-1-phenyl-1*H*-pyrazol-4-yl) methanone (3c). Yield = 71.2% (pale red); m.p. = 240–242 °C. IR: 3296 (NH), 1621 (C=O), 1593 (C=N), 1549 (C=C) cm^{-1}. ^1H NMR δ: 2.47 (s, 3H, CH_3), 2.49 (s, 3H, CH_3), 7.28 (t, J = 7.00 Hz, 1H), 7.44 (d, J = 7.00 Hz, 2H), 7.49–7.52 (m, 5H), 7.55–7.57 (m,

4H), 7.72 (d, J = 8.50 Hz, 2H), 8.10 (s, 1H, pyrazole-H), 13.74 (s, 1H, NH). Mass analysis (m/z, %): 512 (M^+, 16), 429 (13), 428 (22), 416 (14), 270 (29), 170 (22), 163 (100), 148 (24), 95 (29), 88 (40). Analysis for $C_{28}H_{22}ClN_5OS$ (511.12): calculated: C, 65.68; H, 4.33; N, 13.68%. Found: C, 65.60; H, 4.40; N, 13.75%.

3.3 Synthesis of pyrazole 3-hydroxythienyl ketones 5a–c

A mixture of bromoacetyl-pyrazole **1** (1.40 g, 5 mmol), ethyl-3-mercapto-3-(phenylamino)-2-(phenyldiazenyl)acrylate derivative **5a**, **5b**, or **5c** (5 mmol), and triethylamine (0.50 mL) in absolute ethanol (25 mL) was refluxed for three hours. The precipitate formed while heating was filtered, washed with hot ethanol, and dried to yield pyrazolyl 3-hydroxythienyl ketones **5a**, **5b**, and **5c**, respectively.

3.3.1 (3-Hydroxy-5-(phenylamino)-4-(*p*-tolyldiazenyl)thiophen-2-yl)(5-methyl-1-phenyl-1*H*-pyrazol-4-yl)methanone (5a). Yield = 55% (dark red); m.p. = 220–222 °C. IR: 3240 (NH), 1626 (C=O), 1594 (C=N) cm^{-1}. ^1H NMR δ: 2.36 (s, 3H, CH_3), 2.51 (s, 3H, CH_3), 7.30 (d, J = 8.50 Hz, 2H), 7.49–7.58 (m, 10H), 7.75 (d, J = 8.00 Hz, 2H), 8.17 (s, 1H, pyrazole-H), 13.01 (s, 1H, NH). ^{13}C NMR δ: 11.88, 20.57, 101.17, 119.86, 121.42 (2C), 125.15 (4C), 125.86, 128.39, 129.06 (4C), 129.49, 129.65 (4C), 138.98, 138.34, 139.84 (2C), 142.22, 146.29, 153.86. Mass analysis (m/z, %): 493 (M^+, 21), 491 (40), 485 (49), 474 (34), 455 (27), 448 (97), 440 (69), 434 (75), 423 (40), 388 (39), 104 (100). Analysis for $C_{28}H_{23}N_5O_2S$ (493.16): calculated: C, 68.14; H, 4.70; N, 14.19%. Found: C, 68.24; H, 4.78; N, 14.23%.

3.3.2 (3-Hydroxy-4-((4-methoxyphenyl)diazenyl)-5-(phenylamino)thiophen-2-yl)(5-methyl-1-phenyl-1*H*-pyrazol-4-yl) methanone (5b). Yield = 70.8% (red); m.p. = 188–190 °C. IR: 3235 (NH), 1606 (C=O), 1591 (C=N), 1553 (C=C) cm^{-1}. ^1H NMR δ: 2.51 (s, 3H, CH_3), 3.83 (s, 3H, OCH_3), 7.08 (d, J = 8.50 Hz, 2H), 7.30 (t, J = 7.00 Hz, 1H), 7.52–7.57 (m, 9H), 7.92 (d, J = 6.50 Hz, 2H), 8.24 (s, 1H, pyrazole-H), 12.40 (s, 1H, NH). ^{13}C NMR δ: 11.75, 55.30, 100.25, 114.35 (2C), 118.27, 121.27 (2C), 122.25 (2C), 125.05 (3C), 125.60, 128.27, 128.95 (3C), 129.40 (3C), 138.24, 139.65 (2C), 142.09, 152.90, 160.23, 177.39. Mass analysis (m/z, %): 509 (M^+, 51), 493 (39), 489 (35), 485 (34), 472 (44), 433 (41), 375 (72), 339 (49), 326 (84), 325 (86), 289 (53), 285 (75), 284 (100). Analysis for $C_{28}H_{23}N_5O_3S$ (509.15): calculated: C, 66.00; H, 4.55; N, 13.74%. Found: C, 66.08; H, 4.50; N, 13.80%.

3.3.3 (4-((4-Chlorophenyl)diazenyl)-3-hydroxy-5-(phenylamino)thiophen-2-yl)(5-methyl-1-phenyl-1*H*-pyrazol-4-yl) methanone (5c). Yield = 88.1% (dark red); m.p. = 240–242 °C. IR: 3244 (NH), 1596 (C=O), 1532 (C=N), 1521 (C=C) cm^{-1}. ^1H NMR δ: 2.50 (s, 3H, CH_3), 7.31–7.34 (m, 1H), 7.53 (d, J = 4.00 Hz, 4H), 7.54–7.57 (m, 7H), 7.94 (d, J = 8.00 Hz, 2H), 8.21 (s, 1H, pyrazole-H), 12.84 (s, 1H, NH), 13.64 (s, 1H, OH). ^{13}C NMR δ: 11.68, 101.65, 121.29 (4C), 121.53 (4C), 125.00 (4C), 128.90 (5C), 129.08, 129.31 (4C), 132.24, 142.14, 158.25. Mass analysis (m/z, %): 514 (M^+, 27), 492 (14), 484 (14), 481 (39), 478 (36), 473 (62), 471 (12), 446 (40), 445 (100), 424 (20), 355 (28), 341 (14), 231 (23), 205 (37), 189 (15), 139 (37), 125 (36), 99 (34). Analysis for $C_{27}H_{20}ClN_5O_2S$ (513.10): calculated: C, 63.09; H, 3.92; N, 13.63%. Found: C, 63.01; H, 4.07; N, 13.70%.

3.4 Synthesis of pyrazolyl 3-aminothienyl ketones 7a–c

A solution of each 2-cyano-3-mercapto-*N*-phenyl-3-(phenylamino)acrylamide scaffold **7a**, **7b**, or **7c** (5 mmol) and K_2CO_3 (1.38 g, 10 mmol) in dry DMF (25 mL) was stirred at room temperature for 30 minutes. The mixture was then supplemented with 1.40 g of bromoacetyl-pyrazole **1** (5 mmol). For almost six hours, the entire mixture was agitated at 30 °C. The mixture was poured over crushed ice for precipitation. The corresponding pyrazolyl thienyl ketones **7a–c** were produced by filtering, drying, and recrystallizing the resulting powder from an 8 : 1 mixture of ethanol and DMF.

3.4.1 4-Amino-5-(5-methyl-1-phenyl-1*H*-pyrazole-4-carbonyl)-2-(phenylamino)-*N*-(*p*-tolyl)thiophene-3-carboxamide (7a). Yield = 49.8% (yellow); m.p. = 268–270 °C. IR: 3441, 3278 (NH_2, 2NH), 1655, 1630 (2C=O), 1605 (C=N), 1580 (C=C) cm^{-1}. ^1H NMR δ: 2.26 (s, 3H, CH_3), 2.52 (s, 3H, CH_3), 7.12 (d, J = 7.50 Hz, 4H), 7.21 (t, J = 7.50 Hz, 1H), 7.43 (t, J = 7.00 Hz, 2H), 7.49 (d, J = 8.00 Hz, 2H), 7.52–7.56 (m, 5H), 8.38 (s, 1H, pyrazole-H), 8.83 (s, 1H, NH), 9.37 (s, 2H, NH_2), 11.59 (s, 1H, NH). Mass analysis (m/z, %): 507 (M^+, 19), 506 (12), 486 (26), 427 (21), 365 (15), 280 (21), 262 (100), 223 (40), 180 (23), 166 (38), 130 (14), 123 (14), 102 (24), 76 (72). Analysis for $C_{29}H_{25}N_5O_2S$ (507.17): calculated: C, 68.62; H, 4.96; N, 13.80%. Found: C, 68.58; H, 5.00; N, 13.74%.

3.4.2 4-Amino-*N*-(4-methoxyphenyl)-5-(5-methyl-1-phenyl-1*H*-pyrazole-4-carbonyl)-2-(phenylamino)thiophene-3-carboxamide (7b). Yield = 53.6% (orange); m.p. = 218–220 °C. IR: 3403, 3262, 3222 (NH_2, 2NH), 1653, 1635 (2C=O), 1599 (C=N), 1576 (C=C) cm^{-1}. ^1H NMR δ: 2.44 (s, 3H, CH_3), 3.72 (s, 3H, OCH_3), 6.90 (d, J = 9.00 Hz, 2H), 7.37 (s, 4H), 7.47–7.55 (m, 8H), 7.79 (s, 2H, NH_2), 7.99 (s, 1H, pyrazole-H), 9.76 (s, 1H, NH), 9.84 (s, 1H, N–H). ^{13}C NMR δ: 11.68, 55.19, 96.26, 106.08, 113.56 (2C), 114.10, 120.03 (2C), 122.02 (2C), 123.80, 125.36 (2C), 125.48, 128.33, 129.25 (2C), 129.38 (2C), 131.84, 138.67, 138.74, 140.83, 155.50, 155.97, 157.86, 162.07, 178.65. Mass analysis (m/z, %): 523 (M^+, 24), 495 (17), 480 (22), 476 (23), 426 (14), 424 (23), 400 (17), 382 (38), 380 (36), 269 (57), 220 (39), 208 (38), 170 (23), 140 (77), 123 (33), 114 (34), 98 (100), 96 (59). Analysis for $C_{29}H_{25}N_5O_3S$ (523.17): calculated: C, 66.52; H, 4.81; N, 13.38%. Found: C, 67.00; H, 5.70; N, 13.50%.

3.4.3 4-Amino-*N*-(4-chlorophenyl)-5-(5-methyl-1-phenyl-1*H*-pyrazole-4-carbonyl)-2-(phenylamino)thiophene-3-carboxamide (7c). Yield = 62.4% (pale orange); m.p. = 280–282 °C. IR: 3272 (br, NH_2, 2NH), 1640 (br, 2C=O), 1588 (C=N), 1551 (C=C) cm^{-1}. ^1H NMR δ: 2.43 (s, 3H, CH_3), 7.07 (t, J = 6.00 Hz, 1H), 7.36 (d, J = 9.00 Hz, 6H), 7.47 (d, J = 8.00 Hz, 1H), 7.54 (d, J = 4.00 Hz, 4H), 7.69 (d, J = 8.00 Hz, 2H), 7.79 (s, 2H, NH_2), 7.97 (s, 1H, pyrazole-H), 9.93 (s, 1H, NH), 10.17 (s, 1H, NH). ^{13}C NMR δ: 11.68, 96.13, 106.36, 120.18 (2C), 121.03, 121.15, 121.97 (2C), 123.83, 125.12 (2C), 125.45, 126.95, 128.22 (2C), 128.32, 128.82, 129.24 (2C), 129.33 (2C), 138.72 (2C), 140.82, 141.00, 156.40, 162.35. Mass analysis (m/z, %): 528 (M^+, 36), 521 (35), 498 (100), 464 (49), 437 (66), 380 (68), 320 (39), 311 (35), 279 (27), 278 (36), 274 (45), 267 (48), 266 (57), 236 (87), 233 (60), 229 (56), 227 (80), 217 (83), 191 (36), 168 (86). Analysis for

$C_{28}H_{22}ClN_5O_2S$ (527.12): calculated: C, 63.69; H, 4.20; N, 13.26%. Found: C, 63.75; H, 4.29; N, 13.33%.

3.5 Synthesis of pyrazole 3-methylthienyl ketones 9a,b

A solution of each mercapto(phenylamino)methylene derivative **8a** or **8b** (5 mmol) in 25 mL ethyl alcohol and a catalytic quantity of triethylamine (3 drops) was combined with bromoacetylpyrazole **1** (1.40 g, 5 mmol) in a 50 mL single-neck round-bottomed flask. The mixture was refluxed for five hours before being allowed to cool to 30 °C. The corresponding pyrazole-thienyl derivatives **9a** and **9b** were obtained by filtering and recrystallizing the colorful product from the EtOH/DMF mix (10 : 2).

3.5.1 1-(4-Methyl-5-(5-methyl-1-phenyl-1*H*-pyrazole-4-carbonyl)-2-(phenylamino)thio-phen-3-yl)ethan-1-one (9a). Yield = 62.4% (yellow); m.p. = 178–180 °C. IR: 3111 (N–H), 1640, 1608 (2C=O), 1585 (C=N), 1547 (C=C) cm^{-1}. ^1H NMR δ: 2.46 (s, 3H, CH_3), 2.58 (s, 3H, CH_3), 2.63 (s, 3H, CH_3), 7.17–7.20 (m, 1H), 7.43–7.44 (m, 4H), 7.49–7.52 (m, 1H), 7.56–7.57 (m, 4H), 8.07 (s, 1H, pyrazole-H), 11.59 (s, 1H, NH). ^{13}C NMR δ: 11.90, 17.62, 31.48, 119.99, 120.36, 120.69 (2C), 121.73, 125.05 (2C), 125.37, 128.79, 129.46 (2C), 129.94 (2C), 138.43, 139.82, 141.57, 142.97, 143.63, 162.01, 181.53, 196.53. Mass analysis (*m*/*z*, %): 415 (M^+, 23), 398 (15), 396 (16), 390 (15), 382 (63), 350 (20), 309 (43), 299 (77), 298 (46), 294 (44), 278 (54), 275 (37), 270 (28), 252 (55), 242 (40), 239 (20), 219 (27), 215 (19), 116 (59), 85 (100). Analysis for $C_{24}H_{21}N_3O_2S$ (415.14): calculated: C, 69.38; H, 5.09; N, 10.11%. Found: C, 69.31; H, 5.15; N, 10.18%.

3.5.2 Ethyl 4-methyl-5-(5-methyl-1-phenyl-1*H*-pyrazole-4-carbonyl)-2-(phenylamino)-thiophene-3-carboxylate (9b). Yield = 65.7% (brown); m.p. = 150–152 °C. IR: 3139 (N–H), 1640 (2C=O), 1595 (C=N), 1545 (C=C) cm^{-1}. ^1H NMR δ: 1.08 (t, J = 7.00 Hz, 3H, $-COOCH_2\underline{CH_3}$), 2.25 (s, 3H, CH_3), 2.49 (s, 3H, CH_3), 3.95 (q, J = 7.00 Hz, 2H, $-COO\underline{CH_2}CH_3$), 7.32–7.53 (m, 11H), 8.12 (s, 1H, pyrazole-H). ^{13}C NMR δ: 11.41, 14.66, 58.09, 77.51, 104.15, 110.85, 124.49 (2C), 125.33, 128.05, 128.69 (2C), 129.36 (4C), 130.10, 132.52, 137.49, 138.50, 138.89, 139.03, 139.26, 163.75, 167.45. Mass analysis (*m*/*z*, %): 445 (M^+, 40), 435 (57), 418 (39), 399 (44), 368 (81), 337 (100), 287 (64), 268 (75), 263 (74), 240 (22), 227 (40), 221 (35), 208 (38), 187 (55), 143 (37), 95 (55). Analysis for $C_{25}H_{23}N_3O_3S$ (445.15): calculated: C, 67.40; H, 5.20; N, 9.43%. Found: C, 67.23; H, 5.30; N, 9.54%.

3.6 Anticancer activity

3.6.1 Cell cultures. The cell lines MCF-7 and HepG2 were acquired from VACSERA in Cairo, Egypt. The cells were kept in DMEM supplemented with 10% fetal bovine serum, 100 μg per mL streptomycin, and 100 units per mL penicillin. Cells were grown at 37 °C in a humidified environment with 5% CO_2. After a few passes, the cells were planted in a 96-well plate after being cultivated in 75 cm^2 culture bottles with 15 mL DMEM. Cells at 70–80% confluence were used in all investigations.

3.6.2 Cytotoxic assay (MTT assay). A 96-well plate was planted with cancer cell lines (10 000 cells per well). Following a 24 hour cell incubation period, 100 μL of medium containing different concentrations of the chemical (00, 62.5, 125, 250, 500, and 100 μg mL^{-1}) was substituted for the medium for 24 and 72 hours. The control group consisted of untreated cells. The MTT test was used to assess the cell viability following 24 and 72 hours of treatment.[49] The MTT color reaction of mitochondrial dehydrogenase in live cells is the basis of the proliferation test. Each well received MTT (final concentration 5 mg per mL PBS) at the conclusion of the treatment period, and it was then incubated for 2–4 hours at 37 °C in 5% CO_2. 150 μL of DMSO was used to dissolve the colored formazan crystals. A microplate reader was used to measure the absorbance at 570 nm. The percentage of cell proliferation was determined by dividing the absorbance of the treatment group by the absorbance of the control group, then multiplying the result by 100.

3.7 Molecular docking

A common computational tool for comprehending protein–receptor interactions with complexes is molecular docking (MOE2019). By mimicking the exchange of the synthesized chemicals with the breast cancer protein (PDB = 2W3L),[50] the docking process was completed. Only these compounds were exposed to molecular docking due to their increased activity in comparison to the other produced compounds, as determined by the findings of the cytotoxic biological investigation. The builder molecule tool was used to produce ligand compounds, and energy minimization was the next step. Using the MMFF94X force field, this method was repeated until an RMSD gradient of 0.01 kcal mol^{-1} was achieved, with partial charges calculated automatically.

4 Conclusion

Novel pyrazole–thiophene hybrid derivatives were successfully synthesized, and their structures were confirmed by spectral analyses. Biological evaluation demonstrated that several of the synthesized compounds exhibited potent anticancer activity against HepG2 and MCF7 cell lines, highlighting the importance of the pyrazole–thiophene framework in enhancing cytotoxic potential. The observed results suggest that the incorporation of the thiophene moiety into the pyrazole core improves the interaction of the compounds with biological targets and contributes to their antiproliferative effects. Therefore, these hybrids can be considered promising lead compounds for further optimization and development of effective anticancer agents. Besides, the molecular docking study revealed that the synthesized pyrazole thienyl ketones exhibited strong bindings toward the target PDB: 2W3L active site, with most analogues outperforming the vinblastine reference. However, the pyrazole 3-aminothienyl ketones **7a** and **7c** appeared as the most proper analogues due to their highest bindings (−7.1000 and −7.3575 kcal mol^{-1}, respectively) and strong interactions with key residues (Arg105 and Arg66) over multiple bonds such as π–H, π–cation, and different hydrogen bindings with key amino-acid residues. Finally, the *in silico* pharmacokinetic evaluation of the prepared compounds discloses a series with noteworthy challenges but recognizes key structural insights for upcoming optimization. The

predominant limitations are poor solubility and low gastrointestinal absorption, mainly determined by high molecular weight, excessive aromaticity, and high lipophilicity characteristic of the shared molecular scaffold. The existence of the hydrazone linker in both series **3a–c** and **5a–c** correlates with mainly poor profiles. Compound **9a** stands out as the most auspicious lead due to their constructive solubility, acceptable lipophilicity, and high predicted absorption. Future work should focus on synthesizing analogues based on the scaffold of **9a**, aiming to additional reduce CYP inhibition while keeping these higher ADME properties.

Conflicts of interest

There are no conflicts to declare.

Data availability

The data supporting this article have been included as part of the supplementary information (SI). Supplementary information is available. See DOI: https://doi.org/10.1039/d6ra00429f.

References

1 J. S. Brown, S. R. Amend, R. H. Austin, R. A. Gatenby, E. U. Hammarlund and K. J. Pienta, *Mol. Cancer Res.*, 2023, **21**, 1142–1147.
2 B. Liu, H. Zhou, L. Tan, K. T. H. Siu and X.-Y. Guan, *Signal Transduction Targeted Ther.*, 2024, **9**, 175.
3 N. Chatterjee and T. G. Bivona, *Trends Cancer*, 2019, **5**, 170–182.
4 M. Hajimolaali, F. A. Dorkoosh and S. G. Antimisiaris, *J. Liposome Res.*, 2024, **34**, 671–696.
5 N. S. Goud, P. Kumar and R. D. Bharath, *Mini-Rev. Med. Chem.*, 2020, **20**, 1754–1766.
6 D. I. Othman, A. Hamdi, W. M. Elhusseiny, A. S. El-Azab, A. H. Bakheit, M. Hefnawy and A. A.-M. Abdel-Aziz, *Saudi Pharm. J.*, 2023, **31**, 101803.
7 T. J. Price, M. Tang, P. Gibbs, D. G. Haller, M. Peeters, D. Arnold, E. Segelov, A. Roy, N. Tebbutt and N. Pavlakis, *Expert Rev. Anticancer Ther.*, 2018, **18**, 991–1006.
8 F. Bray, M. Laversanne, H. Sung, J. Ferlay, R. L. Siegel, I. Soerjomataram and A. Jemal, *Ca-Cancer J. Clin.*, 2024, **74**, 229–263.
9 P. Koli and R. K. Singh, in *Key Heterocyclic Cores for Smart Anticancer Drug–Design Part II*, Bentham Science Publishers, 2022, pp. 79–104.
10 P. Martins, J. Jesus, S. Santos, L. R. Raposo, C. Roma-Rodrigues, P. V. Baptista and A. R. Fernandes, *Molecules*, 2015, **20**, 16852–16891.
11 M. M. Heravi and V. Zadsirjan, *RSC Adv.*, 2020, **10**, 44247–44311.
12 A. Omar, *Al-Azhar J. Pharm. Sci.*, 2020, **62**, 39–54.
13 E.-J. Hao, Y. Zhao, M. Yu, X.-J. Li, K.-X. Wang, F.-Y. Su, Y.-R. Liang, Y. Wang and H.-M. Guo, *J. Med. Chem.*, 2024, **67**, 12553–12570.
14 B. Kaur, G. Singh, V. Sharma and I. Singh, *Anti-Cancer Agents Med. Chem.*, 2023, **23**, 869–881.
15 F. Zhao, X. Sun, W. Lu, L. Xu, J. Shi, S. Yang, M. Zhou, F. Su, F. Lin and F. Cao, *Drug Delivery*, 2020, **27**, 216–227.
16 H. T. Hamad, *Results Chem.*, 2025, 102182.
17 A. Kumar, A. K. Singh, H. Singh, V. Vijayan, D. Kumar, J. Naik, S. Thareja, J. P. Yadav, P. Pathak and M. Grishina, *Pharmaceuticals*, 2023, **16**, 299.
18 D. K. Lang, R. Kaur, R. Arora, B. Saini and S. Arora, *Anti-Cancer Agents Med. Chem.*, 2020, **20**, 2150–2168.
19 G. Kumari, S. Dhillon, P. Rani, M. Chahal, D. K. Aneja and M. Kinger, *ACS Omega*, 2024, **9**, 18709–18746.
20 S. Singh, S. Tahlan, K. Singh and P. K. Verma, *Curr. Org. Chem.*, 2024, **28**, 325–345.
21 R. A. Mohamed-Ezzat, M. A. Omar, A. Temirak, A. S. Abdelsamie, M. M. Abdel-Aziz, S. A. Galal, G. H. Elgemeie, H. I. El Diwani, K. J. Flanagan and M. O. Senge, *J. Mol. Struct.*, 2024, **1311**, 138415.
22 M. I. Orozco, P. Moreno, M. Guevara, R. Abonia, J. Quiroga, B. Insuasty, M. Barreto, M. E. Burbano and M. d. P. Crespo-Ortiz, *Parasitol. Res.*, 2024, **123**, 75.
23 E. A. Borrego, C. D. Guerena, A. Y. Schiaffino Bustamante, D. A. Gutierrez, C. A. Valenzuela, A. P. Betancourt, A. Varela-Ramirez and R. J. Aguilera, *Cells*, 2024, **13**, 1225.
24 A. I. Alalawy, K. Alatawi, N. A. Alenazi, A. F. Qarah, O. M. Alatawi, R. B. Alnoman, A. Alharbi and N. M. El-Metwaly, *J. Mol. Struct.*, 2024, **1295**, 136609.
25 W. A. Fadaly, A. Elshewy, M. T. Nemr, K. Abdou, A. M. Sayed and N. M. Kahk, *Bioorg. Chem.*, 2024, **152**, 107760.
26 Y. Yu, Y. Zhao, Y. Wang and X. Huang, *J. Chem. Res.*, 2023, **47**, DOI: 10.1177/17475198231202967.
27 R. Murugan, S. R. R. Nayak, B. Haridevamuthu, D. Priya, V. Chitra, B. O. Almutairi, S. Arokiyaraj, M. Saravanan, M. Kathiravan and J. Arockiaraj, *Int. Immunopharmacol.*, 2024, **131**, 111859.
28 M. Rocha, A. Saeed, D. M. Gil, G. A. Echeverría, O. E. Piro, A. Khurshid, M. Arshad, S. A. A. Shah and M. F. Erben, *J. Mol. Struct.*, 2025, **1319**, 139450.
29 Y. Liu, S. Du, X. Xu, L. Qiu, S. Hong, B. Fu, Y. Xiao and Z. Qin, *J. Agric. Food Chem.*, 2024, **72**, 3342–3353.
30 J. Del Gobbo, C. Santini, A. Dolmella, Z. Li, M. Caviglia and M. Pellei, *Molecules*, 2024, **29**, 621.
31 J. Bhagwat and M. Ambre, *International Journal of Multidisciplinary Research*, 2023, **8**, 212–217.
32 R. Shah and P. K. Verma, *Chem. Cent. J.*, 2018, **12**, 137.
33 O. V. Khoroshilova, K. E. Borovkova, L. R. Nikiforova, J. V. Salmova, A. O. Taraskin, D. V. Spiridonova and A. V. Vasilyev, *New J. Chem.*, 2023, **47**, 18492–18516.
34 M. Özgür, M. Yılmaz, H. Nishino, E. Ç. Avar, H. Dal, A. T. Pekel and T. Hökelek, *New J. Chem.*, 2019, **43**, 5737–5751.
35 K. K. Mak, Z. Shiming, O. Epemolu, A. T. Dinkova-Kostova, G. Wells, I. G. Gazaryan, R. Sakirolla, Z. Mohd and M. R. Pichika, *ChemistryOpen*, 2022, **11**, e202200181.
36 A. W. Erian, S. M. Sherif and H. M. Gaber, *Molecules*, 2003, **8**, 793–865.

37 G. E. Said, H. M. Metwally, E. Abdel-Latif, M. R. Elnagar, H. S. Ibrahim and M. A. Ibrahim, *Bioorg. Chem.*, 2024, **151**, 107666.
38 M. R. Elmorsy, E. Abdel-Latif, H. E. Gaffer, S. E. Mahmoud and A. A. Fadda, *Sci. Rep.*, 2023, **13**, 2782.
39 C. J. Goddard, *J. Heterocycl. Chem.*, 1991, **28**, 1607–1612.
40 A. Al-Azmi and E. John, *Text. Res. J.*, 2020, **90**, 2795–2805.
41 M. Metwally, E. Abdel-Latif and F. Amer, *Sulfur Lett.*, 2003, **26**, 119–126.
42 A. H. Harhash, F. A. K. Amer, M. A. F. N. Eldin and M. L. Awad, *Z. Naturforsch., B: J. Chem. Sci.*, 1976, **31**, 846–849.
43 M. Morad, T. M. Habeebullah, I. Althagafi, B. H. Asghar, A. A. Bayazeed, T. M. Bawazeer, A. M. Al-Solimy and N. El-Metwaly, *Res. Chem. Intermed.*, 2020, **46**, 4543–4562.
44 R. M. Mohareb, W. W. Wardakhan and F. I. Hamed, *Med. Chem. Res.*, 2015, **24**, 2043–2054.
45 M. N. Sallam, A. A. Al-Karmalawy, E. M. Abbass, S. S. Hawas, A. M. El-Naggar and A. Hassan, *RSC Adv.*, 2025, **15**, 40078–40092.
46 I. A. El Hassani, S. A. Brandan, A. Altay, E. Yeniceri, A. Alsalme, A. Oulmidi, M. h. Ansar and K. Karrouchi, *J. Mol. Struct.*, 2025, **1324**, 140919.
47 S. Pathania and P. A. Chawla, *Bioorg. Chem.*, 2020, **101**, 104026.
48 A. El-Rayyes, A. S. Almatari, G. E. Abdel-Ghani, A. Saeed and E. Abdel-Latif, *J. Heterocycl. Chem.*, 2023, **60**, 768–780.
49 K. Brusselmans, R. Vrolix, G. Verhoeven and J. V. Swinnen, *J. Biol. Chem.*, 2005, **280**, 5636–5645.
50 S. M. Gomha, S. M. Riyadh, B. Huwaimel, M. E. Zayed and M. H. Abdellattif, *Molecules*, 2022, **27**, 4639.